CaseCrawler: A Lightweight and Low-Profile Crawling Phone Case Robot

Jongeun Lee [ID], Gwang-Pil Jung [ID], Sang-Min Baek [ID], Soo-Hwan Chae [ID], Sojung Yim [ID], Woongbae Kim, and Kyu-Jin Cho [ID]

Abstract—The CaseCrawler is a lightweight and low-profile movable platform with a high payload capacity; it is capable of crawling around carrying a smartphone. The body of the robot resembles a phone case but it has crawling legs stored in its back. It is designed with a deployable, in-plane transmission that is capable of crawling locomotion. The CaseCrawler's leg structure has a knee joint that can passively bend only in one direction; this allows it to sustain a load in the other direction. This anisotropic leg allows a crank slider to be used as the main transmission for generating the crawling motion; the crank slider generates a motion only within a 2D plane. The crank slider deploys the leg when the slider is pushed and retracts it when pulled; this enables a low-profile case that can fully retract the legs flat. Furthermore, by being restricted to swinging within a plane, the hip joint is highly resistant to off-axis deformation, this results in a high payload capacity. As a result, the CaseCrawler has a body thickness of 16 mm (the transmission without the gearbox is only 1.5 mm) and a total weight of 22.7 g; however, it can carry a load of over 300 g, which is 13 times its own weight. To show the feasibility of the robot for use in real-world applications, in this study, the CaseCrawler was employed as a movable platform that carries a 190 g mass, including a smartphone and its cover. This robot can crawl around with the smartphone to enable the phone to charge itself on a wireless charging station. In the future, if appropriate sensing and control functions are implemented, the robot will be able to collect data or return to the owner when needed.

Index Terms—Legged robots, mechanism design, social human-robot interaction, biomimetic, multi-legged robots.

Fig. 1. (a) The CaseCrawler employed as a movable platform. (b) A smartphone with a movable platform moving toward a wireless charging plate by itself.

I. INTRODUCTION

A SMARTPHONE that can move around by itself could potentially offer increased convenience to users. If a smartphone could move around by itself, it could charge itself even if the user forgets to initiate a charge (Fig. 1). Further, it could

be used as a mobile sensor to sense the environment by moving around an area to operate other home appliances, such as an air conditioner or humidifier. It could also bring itself to the user upon request. Several requirements for a mobile robot to be used as a phone case and to transport a phone are as follows: small-scale, lightweight, low-profile, and high payload capacity. Although attaching a mobile robot to a smartphone inherently increases the weight and size, a small, lightweight, and flat design of a robot can minimize degradation of portability. High payload capacity is required to enable the robot to carry a smartphone (typical smartphone weights are up to 200g).

Small-scale and lightweight mobile robots that can crawl have been previously developed, such as HAMR [1]–[6], RoACH [7]–[11], DASH [12], CRAM [13], MutBug [14], and the double-sided CardBot [15]. The smart composite microstructure (SCM) fabrication method [16], which substitutes heavy traditional components with a laminated layer of light materials, has enabled these small, lightweight robots. Moreover, there have been efforts to enhance payload capacity of these robots by implementing a dual-crank design [17], decoupling the load from the leg with a movable platform [18], limiting the off-axis loading of the flexure joints, and reducing the peeling of the
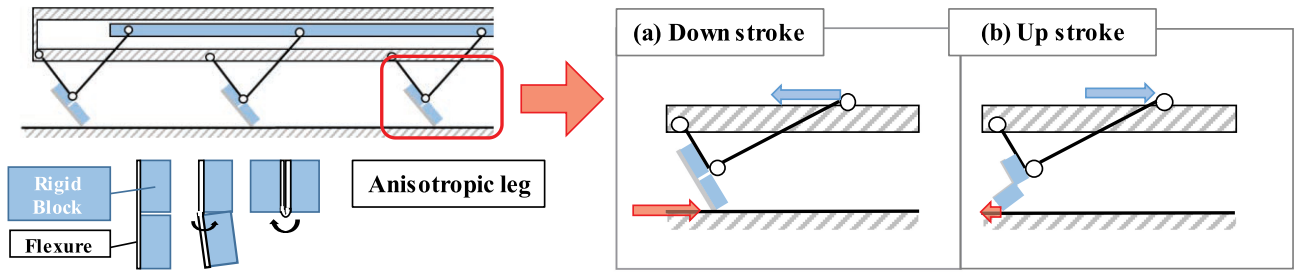
Fig. 2. Running sequence of the crawling robot utilizing the anisotropic legs. The anisotropic leg bends only in a clockwise direction. (a) In the down-stroke, the anisotropic legs become rigid, therefore transmit the force to the ground in the crawling direction. (b) The legs become compliant in the upstroke, so they do not obtain force in the direction opposite of the crawling.

laminated structure through the use of anchoring rivets [19]. The aforementioned SCM-based crawling robots have commonly tried to reduce unwanted deformation by attaching additional structures to increase the payload capacity. All of these efforts have achieved not only small, light structure but also great payload capacity. However, previously developed crawling robots are not flat enough to be attached to a smartphone. In general, crawling requires swing degree of freedom (DoF) for the leg to provide locomotive power and lift DoF to raise the leg from the ground [5]. The combined motion of lifting and swinging requires three-dimensional design of a linkage, which makes the crawling robot bulky. Furthermore, the complicated structure, which has multiple joints, can be easily deformed due to loading. Thus, it is hard to achieve high payload capacity and low-profile at the same time.

In this letter, we propose CaseCrawler: a crawling robot with a form factor of a phone case. The CaseCrawler is lightweight, capable of carrying high payload, and can fully retract its legs at rest. The key design principle is a simplified kinematic chain composed of a crank slider mechanism and deployable leg links with anisotropic leg. Attached to the deployable leg link, anisotropic legs transmit force to the ground only during the downward stroke of the swinging; the knee passively bends during the upstroke to avoid backward force generation, as shown in Fig. 2. Part of the kinematic chain is employed as a crank-slider mechanism to transmit torque from the motor to the rest part of the chain. As a result, the swing motion of the rest part is achieved while repeating protraction and retraction. A low profile is achieved through this deployable linkage, which can be fully retracted at rest. Furthermore, the designed kinematic chain that is allowed to move within a plane permits a high payload capacity by minimizing off-axis deformation of the hip joint.

Based on this design, the proposed CaseCrawler has a body thickness of 16 mm (the transmission without the gearbox is only 1.5 mm) and a payload capacity over 300 g, which is 13 times the robot's own mass. To show the feasibility for use in real-world applications, in this research, the CaseCrawler was employed as a movable platform for a smartphone, as shown in Fig. 1. The robot can continuously operate for 5 minutes at a speed of 2.27 cm/s (0.11 body lengths per second).

The remainder of this paper is organized as follows. First, a design section (Section II) presents the kinematic linkage designed to achieve flat, deployable, and planar leg trajectory.

Section III introduces a model that is used to define and optimize the payload capacity of the crawling locomotion. In Section IV, the model is verified through experiments that measure the reaction force and the crawling speed with varying payloads. Finally, conclusions and plans for future work are presented in Section V.

II. DESIGN

The main challenge in designing the CaseCrawler is to accomplish a crawling locomotion while simultaneously maintaining a low profile and high payload capacity. The lifting motion of the leg required for crawling can be replaced with an anisotropic leg, which can be bent only one way. Therefore, transmission of the crawling robot can be simplified as a single-DoF rotational hip joint to generate the swing motion.

Including the hip joint, the CaseCrawler uses a kinematic chain composed of five links, as shown in Fig. 3. This structure can be actuated within a plane perpendicular to axes of the joints (xy-plane). In order to drive the kinematic chain with a single DoF, a flat slider is constrained in the vertical direction (y-axis), and actuated in the horizontal direction (x-axis). The kinematic chain can be completely flat when pulled by the slider, resulting in a low profile. Furthermore, the restricted DoF of the kinematic chain limits the deformation of the hip joint out of the plane. By preventing deformation, which degrades driving performance of the robot, payload capacity is increased.

The overall configuration of the CaseCrawler is provided in Fig. 3. The robot consists of gearboxes, slider cranks, leg links, and anisotropic legs. Power from an actuator is transmitted through the linkage to generate an output force at the end of the anisotropic legs. The slider moves back and forth in the x-direction to move the leg links in and out, as shown in Figs. 3(a) and 3(b). The anisotropic legs, which can selectively transmit force, are attached to the swinging links to exert force only in the crawling direction. The robot contains two motors (MK07-1.7, DIDEL); each motor is in charge of actuating legs in each side of the robot, and the differential drive of the motors enables the steering of the robot. Three small 3:1 gears are placed in series to minimize the height, resulting in a 27:1 gear ratio. An SCM process, which allows a low-profile structure by laying links and joints on a flat plane, is used to fabricate the robot, as shown in Fig. 4.
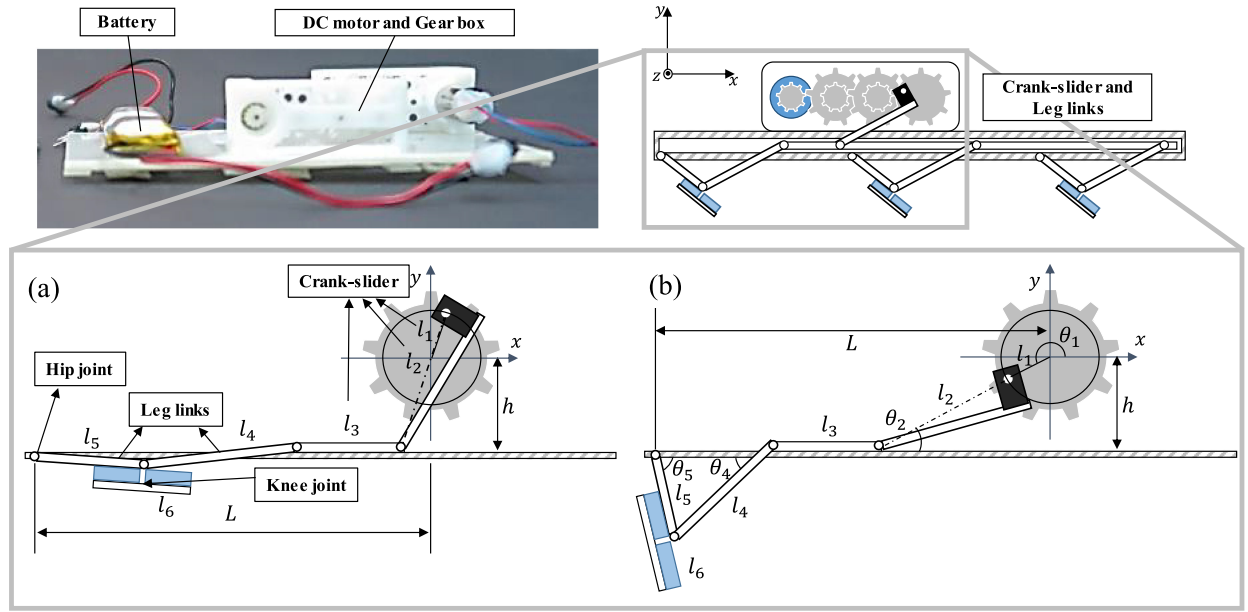
Fig. 3.   Schematics of the crank slider and leg links of the robot. (a) Fully retracted (b) Fully protracted states due to the different angles of the crank.
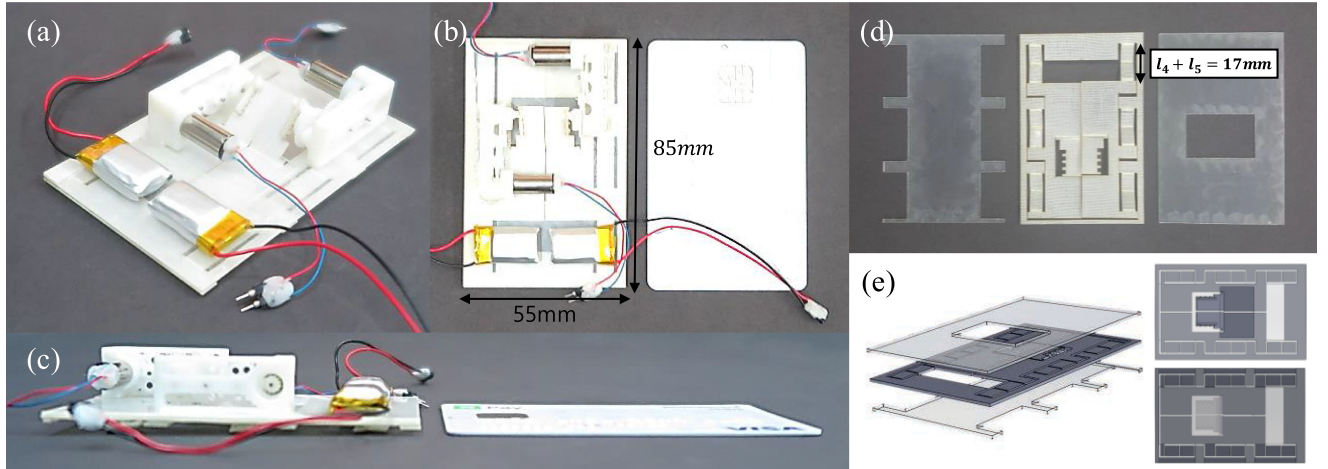

Fig. 4.   (a)–(c) CaseCrawler: A 16 mm high, 23 g crawler with a payload capacity of 300 g. (d) SCM process, which allows a low-profile structure by laying links and joints on a flat plane, is used to fabricate the robot. Main body fabricated by laminating 0.25 um PET and fabric. (e) Three layers are overlaid, where transparent layers on both sides become a linear guide for the slider.

A. Kinematic Chain (Crank Slider and Leg Links)

The kinematic chain, consisting of a crank slider and leg links, is designed to transfer the torque of the motor to the anisotropic leg. The crank slider and the deployable leg links are manufactured from a single laminated sheet composed of PET (0.25T) and fabric, as shown in Fig. 4(d). The slider is stacked between two parallel planes that serve as linear guides for the slider as shown in Fig. 4(e); these guides create a flat sliding motion. As a result, a flat body of 1.5 mm thickness (without the gearbox) in a fully retracted state is developed.

As seen in Figs. 3(a) and 3(b), the slider makes the deployable leg links move in and out. The links are designed to meet kinematic constraints that require the hip joint to have a range

of motion (ROM) from 0 to 90 degrees. The minimum angle is set to 0 degrees to be compact in the initial state; the maximum angle is set to 90 degrees to prevent passing through a singular point. In Fig. 3, the crank slider and the leg links are coupled with the displacement of the slider; thus, they should be considered together. From the two distal conditions of the hip joint angle, the kinematic constraint can be written as

$$l_2 - l_1 = \sqrt{h^2 + (L - l_3 - l_5 - l_4)^2} \qquad (1)$$

$$l_2 + l_1 = \sqrt{h^2 + \left(L - l_3 - \sqrt{l_4{}^2 - l_5{}^2}\right)^2} \qquad (2)$$
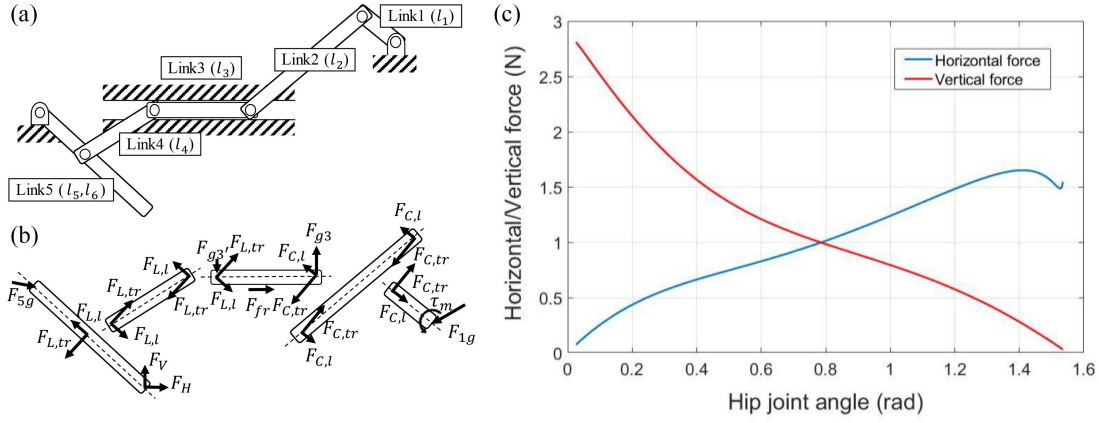
Fig. 5. (a) The transmission of the robot is simplified as a six-bar linkage. (b) Free body diagrams of each link. The links are assumed to be massless, each link must be in force/moment equilibrium. (c) Output force profile according to the hip joint angle is obtained from a kinematic model.

where variables indicate lengths of a crank (l_1), connecting rod (l_2), slider (l_3), leg links (l_4, l_5), height of the body (h), and length between the input gear and hip joint (L), respectively.

B. Anisotropic Leg

Anisotropic legs have been used in many robots to enable an additional DoF via a simple structure [20]–[26]. The proposed anisotropic leg is designed as shown in Fig. 2, where two rigid blocks are attached to a flexure. This compact structure can rotate only in a single direction; the interference between two rigid blocks prevents rotation in the opposite direction. Attached to the swinging leg link, the protracting leg becomes rigid and transmits torque to the ground, while the retracting leg becomes compliant and doesn't transmit the torque. Thus, an anisotropic leg is utilized to prevent backward force that would hinder the propulsion of the robot. This approach helps to achieve a low profile and a high payload capacity by removing the lift DoF of the hip joint, thus simplifying it.

III. MODELING

In this section, payload capacity in crawling locomotion is defined in an inverted pendulum model. From the model, the linkage is optimized to exert force to maximize payload capacity.

Payload capacity in crawling locomotion can be defined as the maximum weight that a mechanism can carry while crawling. To estimate the payload capacity, the simplified template and a specified anchor are considered together [27]. An inverted pendulum model is introduced as a template for obtaining the payload capacity in crawling locomotion. The output force obtained from kinematics of the robot corresponding to the anchor is reflected in the template as a ground reaction force (GRF).

A. Linkage Kinematics (Anchor)

Force generated from a robot's kinematic chain is obtained for the purpose of being substituted into the inverted pendulum model. As shown in Fig. 5(a), the robot is simplified as five links. The output force of the kinematic chain and input motor torque are assumed to be in equilibrium as a quasi-static state.

The force and moment exerted to each link are determined with a free body diagram, as shown in Fig. 5(b). Motor torque is transmitted through the crank and connector (links 1 and 2) to push and pull the slider (link 3). The pushing and pulling force of the slider causes the leg links (links 4 and 5) to protract and retract. As a result, the GRF exerted at the distal end of the leg is calculated from the model. Equations used in Fig. 5(b) include

$$\tau_m = l_1 \, F_{C,tr} \tag{3}$$

$$F_{C,tr} = F_{C,l} \, \tan(\theta_1 - \theta_2) \tag{4}$$

$$F_{L,tr} = F_{L,l} \, tan(\theta_4 + \theta_5) \tag{5}$$

$$(l_5 + l_6) \, F_0 = l_5 \, F_{l,tr} \tag{6}$$

where variables indicate the torque input of the motor (τ_m), the longitudinal/transverse component of force exerted on the crank ($F_{c,l}$, $F_{c,tr}$) and on the leg links ($F_{l,l}$, $F_{l,tr}$), and force at the tip of the leg (F_0).

In order to successfully crawl even in a worst-case condition where only one side of legs are engaged, the input torque is assumed to be the amount of stall torque of a single motor. It is also assumed that only horizontal force is transmitted through the slider, while vertical force generates friction between the slider and the guide for the slider.

Fig. 5(c) represents a modeled profile of the exerted force of the leg according to the corresponding hip joint angle θ_5, when links are designed as $l_4 = l_5 = 8.5$ mm. At a relatively small θ_5, the vertical force is greater than the horizontal force. In contrast, when θ_5 gets larger, the horizontal force becomes greater than the vertical force.

B. Inverted Pendulum Model (Template)

A simplified template for the crawling locomotion can be expressed as an inverted pendulum model that has a concentrated mass above its pivot point [28]. In Fig. 6(a), the crawler is simplified as an inverted pendulum with concentrated mass and a massless leg. Each leg in the model represents three legs on the same side. Since the robot will move slowly around the limit of the payload, locomotion can be expressed as an
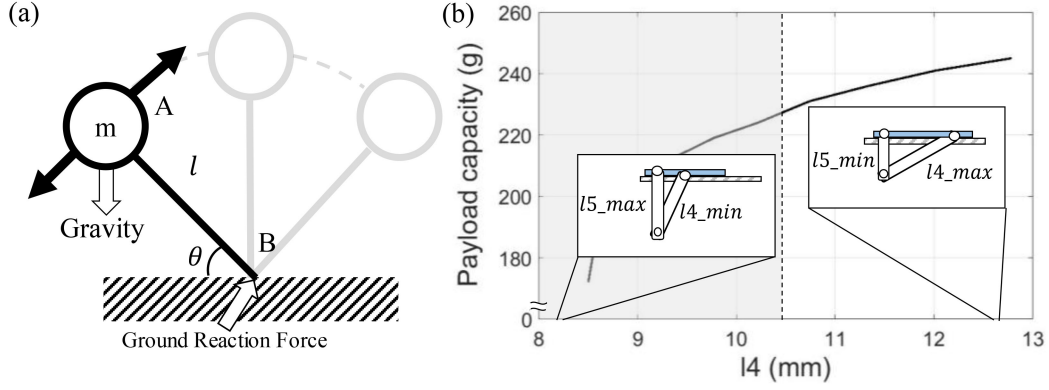
Fig. 6. (a) Inverted pendulum model to obtain the payload capacity. (b) Payload capacity for the given linkage design. The design space indicated as a shaded area has interference between the crank and slider; thus, it is excluded from the design candidates.

inverted pendulum model, rather than as a spring-loaded inverted pendulum model [28], [29].

In the stance phase, the mass rotates around anchored point B. Due to the actuation of the leg, vertical force F_V and horizontal force F_H are exerted from the ground to overcome the gravitational force. The massless legs must transmit the same amount of force from the ground to the center of mass to satisfy the force equilibrium. Dynamics of the mass in the tangential direction can be expressed as below.

$$F_H \sin\theta + F_V \cos\theta - mg\cos\theta = ml\,\ddot{\theta} \qquad (7)$$

where θ represents the angle between the leg and the ground. The mass moves in the tangential direction at an angular velocity $\dot{\theta}$. From (7), the profile of θ under given conditions is obtained to define payload capacity. The payload capacity is defined as the maximum payload in which θ monotonically increases. When the angular velocity becomes negative, crawling locomotion is considered failed due to the payload exceeding capacity.

Since the proposed model simplifies the crawling locomotion into an inverted pendulum model, it can be applied to other crawlers. The profile of the reaction force can be obtained from the kinematics of the transmission of a corresponding crawler. If the deformation of the crawler is not negligible, the effect of any linkage deformation on the force profile should be considered.

C. Design Optimization

Design of the linkage is optimized to maximize the payload capacity by substituting the output force of the linkage into the inverted pendulum model. Among combinations of links that satisfy the kinematic constraints, the most suitable design of the linkage that maximizes the payload capacity is found.

The sum of l_4 and l_5 is constrained as 17 mm, because three legs are aligned in series within a limited design space. The height of the body (h) is fixed as 6.5 mm, slightly larger than the radius of a gear, to define the minimum height. In (1) and (2), by changing l_4 within the design space, the vertical and horizontal force for the corresponding hip joint angle (θ_5) are found. The force profile corresponding to each l_4 is substituted to the inverted pendulum model to figure out whether the crawler

can successfully crawl or not. Results of the modeled payload capacity for the different designs of l_4 are indicated in Fig. 6(b).

Assuming the slider only transmits force in the horizontal direction, the efficiency of the force transmission around the slider determines the output force of the linkage. With a longer l_4, link 4 is nearly horizontal; this means that the sliding force is transmitted effectively. Furthermore, l_1 becomes shorter with a longer l_4; this results in large force transmission from the motor (Eq. (3)). As a result, the payload tends to increase as the length of link 4 increases.

Based on the results, design of the linkage is optimized to exert the force profile that maximizes the payload capacity. The design space indicated as a shaded area in Fig. 6(b) has interference between the crank and slider; thus, it is excluded from the design candidates. Among the feasible candidates, the design of maximum l_4 and minimum l_5 achieves the maximum payload capacity. The maximum payload capacity is obtained as 245 g when the length of link 4 is 12.78 mm.

IV. RESULTS

The following section characterizes performance related to payload capacity of the proposed mechanism. Experiments are performed to measure static and dynamic forces in the vertical and horizontal direction, respectively. Speeds and duty factors at various payloads, steering capability, and obstacle clearances are measured to characterize the performance of the robot as well. Furthermore, to show the potential of the lightweight and low-profile mechanism with high payload capacity, a movable phone case robot is presented as an application.

A. Blocked/Dynamic Force Measurement

A blocked force of the proposed mechanism is measured to validate the output force in a situation similar to carrying a heavy object; thus, it has a small vertical displacement.

For the blocked force measurement, a load cell (Nano17, ATI Industrial Automation) is fixed to a height-adjustable holder above the leg of the inverted robot, as shown in Fig. 7(a). By changing the distance between the load cell and the robot body from 5.7 mm to 8.2 mm, normal force and horizontal force were
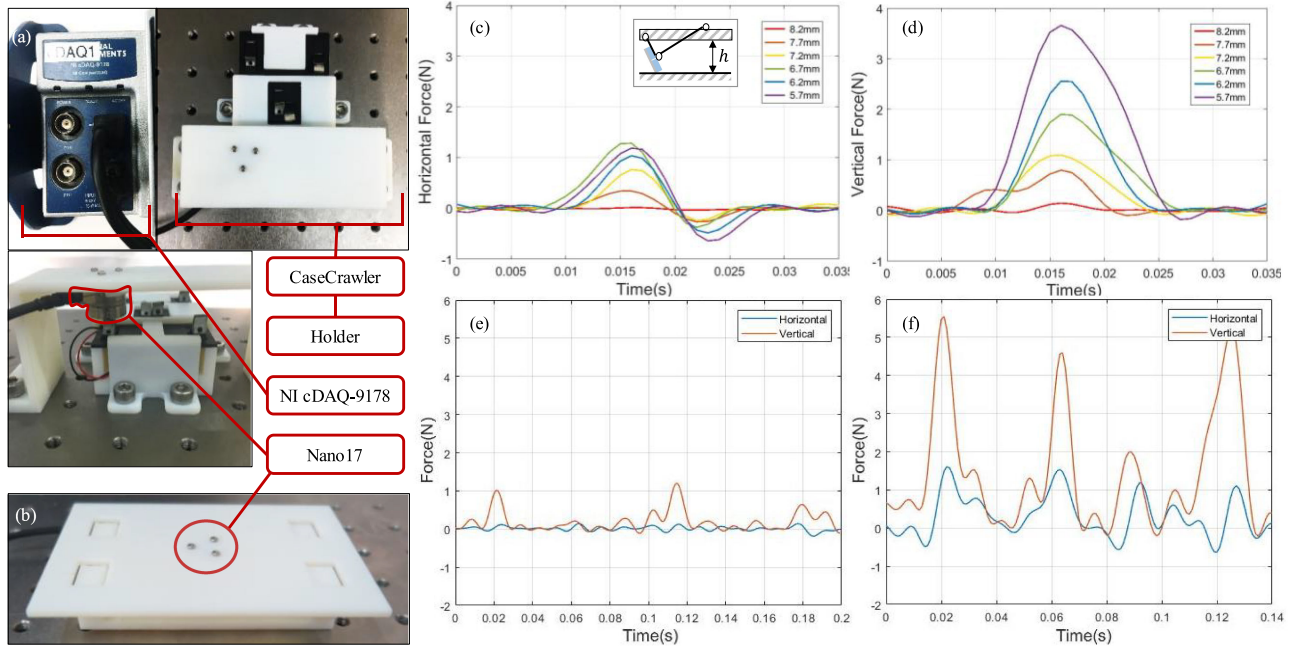
Fig. 7. Experiment for measuring the blocked/dynamic force (a) Experimental setup for measuring the block force. With a distance between the robot and the load cell constrained, horizontal and vertical forces are measured. (b) Experimental setup for measuring the dynamic force. (c), (d) Horizontal/ vertical blocked force measured by varying the distance. (e), (f) Measured dynamic force in the horizontal/vertical direction with 0g payload and 100g payload.

measured as shown in Figs. 7(c) and (d). Results were aligned with respect to the position of the peak to compare the magnitude of the measured force along the distances. For noise cancellation, force data measured 10,000 times per second are filtered by a low-pass FIR filter with a cutoff frequency of 150 Hz (using a 201-point Kaiser window with a beta of 3).

As shown in Figs. 7(c) and (d), the horizontal and vertical forces tend to increase as the distance between the robot and the load cell decreases. Although the tendency agrees with the previous model, the difference occurs mainly because the displacement of the robot in the vertical direction is restricted, which cannot reflect the dynamics of the robot. Furthermore, the leg is forced to be deflected to pass through a narrow gap when the distance between the robot and the load cell gets closer. As the leg bends, the robot engages with the ground with a larger angle of the hip joint, resulting in lower horizontal force and higher vertical force, as shown in the result.

In order to address the limits of the previous experiments, dynamic forces in the horizontal and vertical directions were measured with 0 and 100g payload. As shown in Fig. 7(b), the load cell was positioned below the plate where the crawler passes. The vertical force is measured and shown to be much larger than the horizontal force under high payload. Compared to the blocked force, the vertical force of the dynamic experiment was also shown to be larger. This is mainly because the effect of the payload is also reflected in the result.

B. Running Speed/Duty Factor vs. Payload

The proposed mechanism was characterized with crawling speed for various payloads. The crawler with high loading
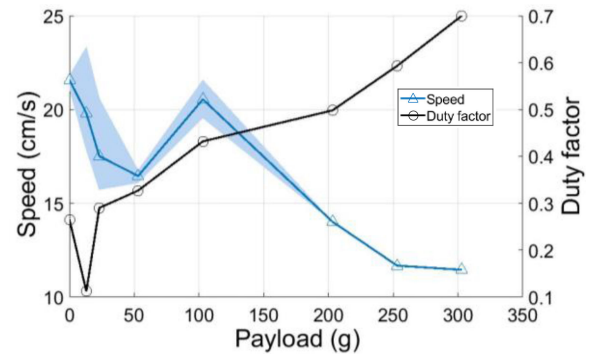

Fig. 8. Results of the speed/duty factor analysis with various payloads. Shaded area indicates the scope of the measurement.

capacity was used for the experiment. The average and range of the measured speeds are indicated in Fig. 8. Speeds were measured three times for each corresponding mass, except for the mass over 200 g, which is a harsh condition for the crawling mechanism.

In the results, the small-scale crawler of 22.7 g was shown to carry up to 303 g, while running at 11.45 cm/s (1.35 body lengths per second). A normalized payload capacity, the ratio between the payload capacity and weight of the robot, was achieved at 13.35, larger than other previously developed robots of similar size (Table I).

When an excessive payload over 300g was applied, the robot failed to lift its body enough to maintain its gait. Crawling while the anisotropic leg remains folded reduces the length of the leg, thus increasing output force and payload capacity.

TABLE I
COMPARISON TO SIMILAR ROBOTS

	CaseCrawler	VelociRoACH [7]	HAMR-VI [6]	VLR [13]	6bar-linkage legged robot [14]
Size (L×W×H) (mm)	85 × 55 × 16	100 × 65 × 42	N/A	155 × 56 × 140	190 × 90 × 70
Speed (cm/s)	21.5	270	9	N/A	40
Mass (g)	22.7	29.1	1.44	149	117.4
Payload capacity (g)	303	125	2.9	400	100
Normalized payload capacity	13.35	4.30	2	2.68	0.85

Fig. 9. Snapshots of the CaseCrawler with 16 mm height overcoming an obstacle of 16 mm height.

Fig. 10. PhoneCaseBot, which consists of a CaseCrawler, a protective shell, and electronics. Mobility is given to the smartphone by attaching a portable crawler with high payload capacity. As a result, the smartphone can crawl to reach the wireless charger.

Furthermore, the linkage formed a closed loop chain structure, which allowed the protraction of the leg links to withstand large loads [30]. However, the crawling speed rapidly dropped due to its inefficient force transmission.

Through further experiments, the duty factor of the mechanism was measured with various payloads. The duty factor was measured by analyzing the engagement and disengagement of anisotropic legs utilizing a high-speed camera. In Fig. 8, the duty factor of the robot is plotted against the payload. Due to the low duty factor in the region of low payload, the robot has a long flight phase, which results in high speed. As the payload increases, the duty factor increases, allowing the robot to provide sufficient force to move heavy loads. However, degradation of the flight phase causes the mechanism to have lower speed.

C. Clearing an Obstacle

To claim the advantage of a crawler that can overcome a relatively high obstacle, we measured the height of an obstacle that the crawler (weight of 23 g, height of 16 mm, and leg length of 11.1 mm) presented in Fig. 4 can overcome. The book used in the experiment is 16 mm high, which is similar to the CaseCrawler height, as shown in Fig. 9. After a few trials, the robot overcame the obstacle. In spite of its low profile, the crawler overcame the obstacle by utilizing its bouncing gait.

D. Steering

The proposed mechanism is able to steer by the differential drive of two motors. By actuating a single motor at a time, the turning rate and turning radius are measured for left and right steering. Tests were conducted five times in each direction. When turning to the right, the turning rate was 1.36 rad/s and the radius was 5.88 cm. Turning in the opposite direction results in 1.04 rad/s and 4.8 cm of turning rate and radius, respectively.

E. Application – PhoneCaseBot

Utilizing the advantages of the high payload capacity and the low profile of the proposed mechanism, a movable platform for a smartphone was designed, as shown in Fig. 10. A smartphone capable of wireless charging (Galaxy S6 edge+, Samsung, 153g) was selected to be given mobility. The movable platform consists of an enlarged version of the CaseCrawler and an outer shell printed by a 3D printer (DM_8520_Grey40, Objet 260 Connex, Stratasys) to protect the smartphone. Also, a receiver (jf24sv), a motor driver (HR8833), and batteries (LiPo, 3.7V, 85 mAh) were used to receive the control signals from the controller. Platform dimensions are 205 × 82.5 × 24 mm; weight is 81.55 g without the smartphone. As shown in Fig. 1(b), after reaching the charging spot, the platform stops moving, allowing phone charging. The platform attached under the smartphone has a low profile; thus, the distance between the phone and the charger is within the chargeable range in the vertical direction.

V. CONCLUSION

Here, we present a low-profile, lightweight movable platform with high payload capacity that utilizes a flat structure with a deployable anisotropic leg. In addition, we propose a method of obtaining high payload capacity by applying the force profile of the linkage to the inverted pendulum model; this is used to optimize the linkage. As a result, our crawling mechanism of 22.7 g can carry a load up to 303 g, 13.35 times its weight. By enlarging the crawling mechanism, a platform was developed to allows a smartphone to reach a wireless charging pad.

In order to extend the platform into a system, further movable platforms optimized for various objects will be made in future work. In addition, future development of autonomous control of the platform with sensing capability will expand the usability of it. One possible solution is for the robot to share the sensors, controller, and power of the smartphone [31]. When the crawling mechanism becomes autonomous, the scope of tasks that can be performed can also be expanded.

Another potential application of this movable platform is to move attached sensors for mapping acquired data, or to move cameras to take photos in the places inaccessible to the user. As these proposed applications show, mobility widens the working range of the objects, which reduces the physical distance and enhances the interactions between the objects.

REFERENCES

[1] A. T. Baisch and R. J. Wood, "Pop-up assembly of a quadrupedal ambulatory microrobot," in *Proc. IEEE Int. Conf. Intell. Robots Syst.*, 2013, pp. 1518–1524.

[2] A. T. Baisch, "Design, manufacturing, and locomotion studies of ambulatory micro-robots," Ph.D. dissertation, School Eng. Applied Sci., Harvard Univ., Cambridge, MA, USA, 2013.

[3] K. Jayaram, J. Shum, S. Castellanos, E. F. Helbling, and R. J. Wood, "Scaling down an insect-size microrobot, HAMR-VI into HAMR-Jr," 2020, *arXiv: 2003.03337*.

[4] O. Ozcan, A. T. Baisch, D. Ithier, and R. J. Wood, "Powertrain selection for a biologically-inspired miniature quadruped robot," in *Proc. IEEE Int. Conf. Robot. Autom.*, 2014, pp. 2398–2405.

[5] A. T. Baisch, C. Heimlich, M. Karpelson, and R. J. Wood, "HAMR3: An autonomous 1.7 g ambulatory robot," in *Proc. IEEE Int. Conf. Intell. Robots Syst.*, 2011, pp. 5073–5079.

[6] N. Doshi, B. Goldberg, R. Sahai, N. Jafferis, D. Aukes, and R. J. Wood, "Model driven design for flexure-based microrobots," in *Proc. IEEE Int. Conf. Intell. Robots Syst.*, 2015, pp. 4119–4126.

[7] A. M. Hoover, E. Steltz, and R. S. Fearing, "RoACH: An autonomous 2.4 g crawling hexapod robot," in *Proc. IEEE Int. Conf. Intell. Robots Syst.*, 2008, pp. 26–33.

[8] D. W. Haldane, K. C. Peterson, F. L. G. Bermudez, and R. S. Fearing, "Animal-inspired design and aerodynamic stabilization of a hexapedal millirobot," in *Proc. IEEE Int. Conf. Robot. Autom.*, 2013, pp. 3279–3286.

[9] D. W. Haldane and R. S. Fearing, "Running beyond the bio-inspired regime," in *Proc. IEEE Int. Conf. Robot. Autom.*, 2015, pp. 4539–4546.

[10] G. P. Jung *et al.*, "JumpRoACH: A trajectory-adjustable integrated jumping-crawling robot," *IEEE/ASME Trans. Mechatronics*, vol. 24, no. 3, pp. 947–958, Jun. 2019.

[11] A. O. Pullin, N. J. Kohut, D. Zarrouk, and R. S. Fearing, "Dynamic turning of 13cm robot comparing tail and differential drive," in *Proc. IEEE Int. Conf. Robot. Autom.*, 2012, pp. 5083–5093.

[12] P. Birkmeyer, K. Peterson, and R. S. Fearing, "DASH: A dynamic 16 g hexapedal robot," in *Proc. IEEE Int. Conf. Intell. Robots Syst.*, 2009, pp. 2683–2689.

[13] K. Jayaram and R. J. Full, "Cockroaches traverse crevices, crawl rapidly in confined spaces, and inspire a soft, legged robot," *Proc. Nat. Acad. Sci. USA*, vol. 113, no. 8, pp. E950–E957, 2016.

[14] T. Y. Kim, C. Kim, S. H. Kim, and G. P. Jung, "MutBug: A lightweight and compact crawling robot that can run on both sides," *IEEE Robot. Autom. Lett.*, vol. 4, no. 2, pp. 1409–1415, Apr. 2019.

[15] J. E. Lee, G. P. Jung, and K. J. Cho, "Bio-inspired design of a double-sided crawling robot," in *Proc. Conf. Biomimetic Biohybrid Syst.*, 2017, vol. 10384, pp. 562–566.

[16] R. J. Wood, S. Avadhanula, R. Sahai, E. Steltz, and R. S. Fearing, "Microrobot design using fiber reinforced composites," *J. Mech. Des.*, vol. 130, no. 5, 2008, Art. no. 052304.

[17] C. S. Casarez and R. S. Fearing, "Steering of an underactuated legged robot through terrain contact with an active tail," in *Proc. IEEE Int. Conf. Intell. Robots Syst.*, 2018, pp. 2739–2746.

[18] D. Yun and R. S. Fearing, "VLR: Cockroach millirobot with load decoupling structure," in *Proc. IEEE Int. Conf. Adv. Intell. Mechatronics*, 2015, pp. 127–132.

[19] D. Yun and R. S. Fearing, "Cockroach milli-robot with improved load capacity," *J. Mech. Des.*, vol. 11, no. 3, pp. 1–12, 2019.

[20] J. S. Lee and R. S. Fearing, "Anisotropic collapsible leg spines for increased millirobot traction," in *Proc. IEEE Int. Conf. Robot. Autom.*, 2015, pp. 4547–4553.

[21] A. Rafsanjani, Y. Zhang, B. Liu, S. M. Rubinstein, and K. Bertoldi, "Kirigami skins make a simple soft actuator crawl," *Sci. Robot.*, vol. 3, no. 15, 2018, Art. no. eaar7555.

[22] J.-S. Koh and K.-J. Cho, "Omega-shaped inchworm-inspired crawling robot with large-index-and-pitch (LIP) SMA spring actuators," *IEEE/ASME Trans. Mechatronics*, vol. 18, no. 2, pp. 419–429, Apr. 2013.

[23] A. Firouzeh, T. Higashisaka, K. Nagato, K. J. Cho, and J. Paik, "Stretchable Kirigami components for composite meso-scale robots," *IEEE Robot. Autom. Lett.*, vol. 5, no. 2, pp. 1883–1890, Apr. 2020.

[24] M. A. Skylar-Scott, J. Mueller, C. W. Visser, and J. A. Lewis, "Voxelated soft matter via multimaterial multinozzle 3D printing," *Nature*, vol. 575, no. 7782, pp. 330–335, 2019.

[25] Y. Wu *et al.*, "Insect-scale fast moving and ultrarobust soft robot," *Sci. Robot.*, vol. 4, no. 32, 2019, Art. no. eaax1594.

[26] X. Ji *et al.*, "An autonomous untethered fast soft robotic insect driven by low-voltage dielectric elastomer actuators," *Sci. Robot.*, vol. 4, no. 37, 2019, Art. no. eaaz6451.

[27] P. Holmes, R. J. Full, D. Koditschek, and J. Guckenheimer, "The dynamics of legged locomotion: Models, analyses, and challenges," *SIAM Rev.*, vol. 48, no. 2, pp. 207–304, 2006.

[28] S. Kajita, F. Kanehiro, K. Kaneko, K. Fujiwara, K. Yokoi, and H. Hirukawa, "Biped walking pattern generation by a simple three-dimensional inverted pendulum model," *Adv. Robot.*, vol. 17, no. 2, pp. 131–147, 2003.

[29] M. H. Dickinson, C. T. Farley, R. J. Full, M. Koehl, R. Kram, and S. Lehman, "How animals move: an integrative view," *Science*, vol. 288, no. 5463, pp. 100–106, 2000.

[30] Y. Pan and F. Gao, "Payload capability analysis of a new kind of parallel leg hexapod walking robot," in *Proc. Int. Conf. Adv. Mechatronic Syst.*, 2013, pp. 541–544.

[31] G. Loianno *et al.*, "Autonomous flight and cooperative control for reconstruction using aerial robots powered by smartphones," *Int. J. Rob. Res.*, vol. 37, no. 11, pp. 1341–1358.